# On the velocity distributions of the one-dimensional inelastic gas

**A Barrat**[1], **T Biben**[2], **Z Rácz**[1,3], **E Trizac**[1] **and F van Wijland**[1]

[1] Laboratoire de Physique Théorique, Université de Paris-Sud, 91405 Orsay Cedex, France
[2] Laboratoire de Spectrométrie Physique, Bâtiment 45, Avenue de la Physique, Domaine
Universitaire, BP 87, 38402 Saint Martin d'Heres, France
[3] Institute for Theoretical Physics, Eötvös University, Pázmány sétány 1/a, 1117 Budapest,
Hungary

**Abstract**
We consider the single-particle velocity distribution of a one-dimensional fluid
of inelastic particles. Both the freely evolving (cooling) system and the
non-equilibrium stationary state obtained in the presence of random forcing
are investigated, and special emphasis is paid to the small inelasticity limit.
The results are obtained from analytical arguments applied to the Boltzmann
equation along with three complementary numerical techniques (molecular
dynamics, direct Monte Carlo simulation methods and iterative solutions
of integro–differential kinetic equations). For the freely cooling fluid, we
investigate in detail the scaling properties of the bimodal velocity distribution
emerging close to elasticity and calculate the scaling function associated with
the distribution function. In the heated steady state, we find that, depending
on the inelasticity, the distribution function may display two different stretched
exponential tails at large velocities. The inelasticity dependence of the
crossover velocity is determined, and it is found that the extremely high-velocity
tail may not be observable at 'experimentally relevant' inelasticities.

PACS numbers: 05.70.Ln, 02.70.Ns, 02.70.Uu, 05.10.Ln

## 1. Introduction

### 1.1. Motivation

In the widely studied context of non-equilibrium stationary states, granular gases stand out as
an interesting model system, accessible to and the subject of many experimental and analytic
investigations. Their theoretical description and understanding is one of the present important
issues of the development of the out-of-equilibrium statistical mechanics.

The main difference between molecular gases and granular gases stems from the fact that at each collision between, e.g., steel or glass beads (in experiments), or idealized smooth hard spheres (in analytical and numerical investigations), a fraction of the relative kinetic energy is lost [1]. This inelasticity is responsible for many interesting phenomena, such as the appearance of spatial heterogeneities, non-Gaussian velocity distributions, etc. Theoretically, two opposite situations have been extensively studied in the context of smooth inelastic hard spheres we shall consider here, namely, the free cooling case where no forcing mechanism compensates the energy loss due to dissipative collisions (see, e.g., the review [2] and references therein), and the uniformly heated system where an external random force acts as a heating process on the grains, allowing a non-equilibrium stationary state to be reached [3–5].

In this paper, we will study the above two situations (i.e. with or without energy input), and concentrate on a one-dimensional granular fluid. For the homogeneously heated gas (section 2), the focus will be on the high-energy tail of the velocity distribution $P(v)$. Whereas the velocities up to the thermal scale obey a Maxwell–Boltzmann-like distribution, we will show by combining kinetic theory arguments and numerical simulations (both molecular dynamics (MD) and Monte Carlo) that in the limit of vanishing inelasticity, $P(v)$ displays an $\exp(-v^3)$ large $v$ behaviour. At finite inelasticity, this tail is asymptotically dominated by the $\exp(-v^{3/2})$ law already predicted in [4]. These predictions will also be confirmed by the results of a high-precision iterative solution of the non-linear Boltzmann equation. On the other hand, without energy injection (section 3), we will similarly concentrate on the limit of small inelasticity (that appears quite singular, unlike in the heated case), and shed some light on the importance of spatial heterogeneities and velocity correlations: detailed scaling properties of the solutions of the homogeneous Boltzmann equation will be obtained analytically and checked numerically. Further confrontation against molecular dynamics simulations will show that the velocity distributions of the Boltzmann homogeneous cooling state share some common features with those obtained by integrating the exact equations of motion.

## 1.2. The model

We shall consider a one-dimensional gas of equal mass particles of length $\sigma$ and density $n$, evolving on a line of length $L = N/n$ with periodic boundary conditions. These particles undergo binary collisions with conservation of momentum but loss of a fraction $(\alpha^2)$ of the kinetic energy in the centre-of-mass frame: consequently, if $v_1$ and $v_2$ (respectively $v'_1$ and $v'_2$) are the velocities of the two particles involved before (respectively after) the collision, then

$$v'_1 + v'_2 = v_1 + v_2 \tag{1}$$
$$v'_1 - v'_2 = -\alpha(v_1 - v_2) \tag{2}$$

where $0 \leqslant \alpha \leqslant 1$ is the restitution coefficient. We also introduce the inelasticity parameter $\varepsilon = 1 - \alpha$ ($\varepsilon = 0$ for elastic collisions).

We will focus on the behaviour of the velocity distribution $P(v, t)$ in the following two cases:

- Without energy injected, the above collision rules define a system where energy dissipation through collisions is not balanced and the typical velocities of particles progressively decrease. This free cooling regime has been widely studied [6–19] and in particular in dimension 1 by molecular dynamics studies [6, 7, 9, 19]. Slight modifications of the collision rule allow us to bypass the inelastic collapse [20] and observe an asymptotic scaling regime for $P(v, t)$ [19].

- A steady state can be reached if the loss of energy through collisions is balanced by an injection that can be achieved through a random force $\eta(t)$ acting on each particle,

$$\frac{\mathrm{d}v}{\mathrm{d}t} = F + \eta(t) \qquad \langle \eta(t)\eta(t')\rangle = 2D\delta(t - t') \tag{3}$$

where $D$ is the amplitude of the injected power and $F$ the systematic force due to inelastic collisions. Velocities consequently execute a random walk between the collisions, and in the collisionless case $P(v, t)$ obeys a diffusion equation with a 'diffusion' coefficient $D$. This model was first introduced and discussed by Williams and MacKintosh [3] in dimension 1, and studied in higher dimensions [5]; variants have also been proposed [21, 22].

We define the granular temperature as the average kinetic energy of the system:

$$T(t) = \int \mathrm{d}v \, v^2 P(v, t). \tag{4}$$

The function $T(t)$ decreases for the freely cooling system, but it eventually fluctuates around a steady-state value in the heated case.

### 1.3. Investigation methods

Our study relies on the following three complementary approaches:

- Molecular dynamics (MD) simulations [23] integrate the exact equations of motion in a finite box: we consider $N$ hard rods of length $\sigma$, on a line of linear size $L$, with periodic boundary conditions and random initial velocities, and we use an event-driven algorithm to study their dynamics.
- The Boltzmann equation describes the evolution of the one-particle distribution function $P(v, t)$, upon the molecular chaos factorization hypothesis [24]. This equation is therefore a mean-field approximation of the problem, in which density becomes irrelevant. It can be solved numerically by the direct simulation Monte Carlo (DSMC) method [25], or in certain cases, with an even better precision, by an iterative method similar to that used in [26].
- In the elastic limit $\alpha \to 1$, an analytical scaling approach can be used to study the Boltzmann equation. It is important to note that, in the particular case of one-dimensional hard spheres, the elastic case $\varepsilon = 0$ is quite peculiar. Indeed, for $\varepsilon = 0$, the collisions only exchange the velocities of the particles: this system is therefore unable to thermalize and is equivalent to one with transparent particles where $P(v, t)$ is frozen in time.

## 2. Steady state of the heated fluid

The exact solution of the problem of a $d = 1$ inelastic gas appears inaccessible, which prompted us to carry out MD simulations to calculate $P(v, t)$. In order to see whether a mean-field-type approach can give a reasonable description of the inelastic gas, we reconsider the kinetic theory of the process. We solve the appropriate Boltzmann equation by simulations in the general $\alpha$ case, and derive exact results in the $\varepsilon \to 0$ limit.

Since the gas systematically reaches a stationary state with a temperature $T$ that depends on the inelasticity (see below), it is useful to introduce the rescaled velocity
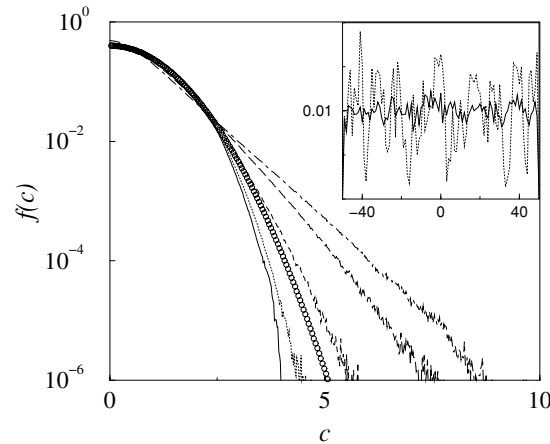
$$c = \frac{v}{\sqrt{T}} \tag{5}$$

**Figure 1.** Velocity distributions for MD simulations with 5000 particles, density $n\sigma = 0.5$, for restitution coefficients 0.6, 0.9, 0.95, 0.99 and 0.999 (from top to bottom). The symbols show the Gaussian distribution. The inset shows a typical snapshot of the space density fluctuations for 0.99 (continuous line) and 0.6 (dotted line).

and the corresponding distribution function

$$f(c) = \sqrt{T(t)}P(v, t). \tag{6}$$

In order to compare the velocity distributions at various inelasticities, numerical data for the *rescaled velocity* distributions will always be displayed in the figures.

### 2.1. General $\alpha$ case

*2.1.1. Molecular dynamics simulations.* The molecular dynamics simulations are carried out with $N = 5000$ hard rods, using an event-driven algorithm, and submitting the rods to random kicks at a frequency that remains much higher than the collision frequency, in order to simulate the noise of equation (3). Note that, since the Langevin equation considered in [21] is different from ours[4], comparing the two approaches is not possible without further investigations on either side.

Starting from an initial distribution of velocities, a steady state is reached after a transient, and velocity distributions can be measured. Figure 1 displays such distributions for inelasticity ranging from $\alpha = 0.6$ to 0.999. Strong non-Gaussian behaviour is observed, with over- or under-populated high-energy tails depending on $\alpha$. Moreover, the inset shows that the system remains quite homogeneous at low inelasticity, while strong density fluctuations develop at larger inelasticity. The value of the density $n$ of the system seems to have no influence on the shape of the velocity distributions, and density fluctuations seem to increase roughly proportional to $1/(n\sigma)$ (at constant $\alpha$). Detailed investigations of the spatial correlations are left for future studies.

*2.1.2. Kinetic theory.* Assuming that the density of the particles is low and neglecting both velocity and spatial correlations of colliding partners, the Boltzmann equation for the spatially

---

[4] It contains a friction term in velocity space whose amplitude is linked to the force amplitude, whereas detailed balance is not satisfied by our model, where the forcing is independent of the state of the system. We did not consider the friction term in order to study a model (leading to a steady state) with a minimal number of parameters.

averaged velocity distribution function $P(v, t)$ can be written as [7, 15]

$$\partial_t P - D\partial_v^2 P = -n \int_{-\infty}^{\infty} \mathrm{d}v' |v - v'| P(v) P(v')$$

$$+ \frac{4n}{(1+\alpha)^2} \int_{-\infty}^{\infty} \mathrm{d}v' |v - v'| P(v') P\left(\frac{2v - (1-\alpha)v'}{1+\alpha}\right). \quad (7)$$

The right-hand side of equation (7) contains the collision terms corresponding to the 'dissipative' rules (2), while the Fokker–Planck term $D\partial_v^2 P$ on the left-hand side takes into account the energy injected by the random forces (3).

The system described by equation (7) is expected to relax to a steady state since the power input is independent of the velocities while the loss of energy is roughly proportional to the energy itself. This expectation can be made more quantitative by deducing the equation for the temperature ($T = \langle v^2 \rangle$) of the system

$$\frac{\mathrm{d}\langle v^2 \rangle}{\mathrm{d}t} = 2D - \frac{n}{4}(1-\alpha^2)\langle |v - v'|^3 \rangle \quad (8)$$

where $\langle \cdots \rangle$ denotes averaging with $P(v, t)$ and $|v - v'|$ represents the relative velocity of two randomly chosen particles. There is a stationary solution to this equation that has a simple physical meaning. Namely, the rate of input of energy ($\sim D$) is equal to the rate of loss of kinetic energy in the centre-of-mass frame $\sim (1 - \alpha^2)(v - v')^2$ (with the extra factor $n|v - v'|$ coming from the collision rate). One may also estimate the characteristic time of reaching the steady state. Indeed, the quantities $T^{3/2} = \langle v^2 \rangle^{3/2}$ and $\langle |v|^3 \rangle$ are expected to have the same leading large-time ($t \to \infty$) dependence, and thus, up to an unknown numerical constant $\mathcal{C}$, equation (8) can be written as

$$\frac{\mathrm{d}T}{\mathrm{d}t} = 2D - \mathcal{C} \, n(1-\alpha^2)T^{3/2}. \quad (9)$$

The typical relaxation time is then $\tau_{\text{relax}} \sim [D/(n(1 - \alpha^2))]^{2/3}$. In the small inelasticity limit ($\varepsilon \to 0$), this relaxation time diverges as $\tau_{\text{relax}} \sim \varepsilon^{-2/3}$. We have indeed observed such a behaviour of the approach to the steady state in both MD and DSMC simulations.

Many pieces of information on the stationary distribution function have been obtained in [4]; in particular, the deviations from a Gaussian $\Phi(c) = \mathrm{e}^{-c^2/2}/\sqrt{2\pi}$ have been investigated by the Sonine expansion [27]

$$f(c) = \Phi(c) \left(1 + \sum_{p=1}^{\infty} a_p S_p(c^2)\right) \quad (10)$$

where $S_p$ are polynomials orthogonal with the Gaussian weight $\Phi$. The coefficients $a_p$ are then obtained from the moments of $f$. From the definition of temperature, $a_1$ vanishes and the first correction $a_2$, which is related to the kurtosis of the velocity distribution, has been computed in any dimension neglecting non-linear contributions of $\mathcal{O}(a_2^2)$; in dimension 1, it has the expression

$$a_2 \equiv 4\left(\frac{\langle v^4 \rangle}{3\langle v^2 \rangle^2} - 1\right) = \frac{16(1 - 2\alpha^2)}{129 + 30\alpha^2}. \quad (11)$$

We note a peculiarity of dimension 1: $a_2$ does not vanish as $\alpha \to 1$, unlike in space dimensions $d > 1$ in which $\lim_{\alpha \to 1} a_2 = 0$. This is a hint that the quasi-elastic limit is more singular in $d = 1$ than in higher dimensions.

Besides, it was shown in [4] how to determine the high-energy tail of the velocity distribution. We briefly recall the argument. The $\varepsilon$-dependent gain term in the collision

integral appearing in the Boltzmann equation (7) is *a priori* neglected. In the large velocity limit the resulting equation for the steady-state distribution $P_s(v)$ reads

$$D\frac{\mathrm{d}^2 P_s}{\mathrm{d}v^2} = -n|v|P_s(v) \tag{12}$$

which yields a high-energy tail of the form $\exp\left(-\frac{2}{3}\sqrt{n/D}|v|^{3/2}\right)$. Then one verifies that the gain term is indeed negligible (as would be the case for any solution decaying faster than exponentially). The 3/2 exponent is independent of the space dimension; therefore the behaviour of the large-$c$ tail is singular for $\varepsilon \to 0$, with an exponent jumping abruptly from 3/2 for $\varepsilon > 0$ to 2 for $\varepsilon = 0$ (for dimensions larger than 1, the elastic system equilibrates and thus $f$ is a Gaussian).

*2.1.3. Numerical solution of the homogeneous Boltzmann equation.* We have obtained numerically the exact solution of the Boltzmann equation, i.e. the velocity distributions, in the homogeneous situation, for various values of the restitution coefficient. Two methods have been used: the well known DSMC method and another powerful iterative method, recently introduced by Biben *et al* [26]. Let us recall the idea of this method.

The stationary velocity distribution can be obtained numerically through a direct iteration of equation (7). From an initial guess for the velocity distribution $P(v)$ (a step function for example), the time evolution can be computed from equation (7) until the steady state is reached. Taking advantage of the $v \to -v$ symmetry of the velocity distribution, we only need to know the values of $P$ for positive velocities. $P(v)$ is then discretized from $v = 0$ to $v = (N_v - 1)\mathrm{d}v$, where typically $N_v = 1000$ and $\mathrm{d}v = 0.01\sqrt{D\sqrt{\pi}/(n(1-\alpha^2))}$. The right-hand side of equation (7) can be estimated using the Simpson integration, combined with a quadratic interpolation method to estimate the values of

$$P\left(\frac{2v - (1-\alpha)v'}{1+\alpha}\right)$$

whose argument does not necessarily coincide with the velocity discretization. An implicit method is used to solve the diffusion equation: if $P_i^{t+\mathrm{d}t}$ denotes the new estimate of $P(i\,\mathrm{d}v)$ at time $t + \mathrm{d}t$, the left-hand side of equation (7) can be written in the time–velocity discretized space:

$$\frac{\mathrm{d}P}{\mathrm{d}t} - D\partial_v^2 P \to \frac{P_i^{t+\mathrm{d}t} - P_i^t}{\mathrm{d}t} - D\frac{P_{i+1}^{t+\mathrm{d}t} - 2P_i^{t+\mathrm{d}t} + P_{i-1}^{t+\mathrm{d}t}}{\mathrm{d}v^2}$$

which leads to the following equation for $P_i^{t+\mathrm{d}t}$:

$$\left(1 + 2D\frac{\mathrm{d}t}{\mathrm{d}v^2}\right)P_i^{t+\mathrm{d}t} - D\frac{\mathrm{d}t}{\mathrm{d}v^2}\left(P_{i+1}^{t+\mathrm{d}t} + P_{i-1}^{t+\mathrm{d}t}\right) = P_i^t + \mathrm{d}t\{\text{RHS of (7) at site } i \text{ and time } t\}. \tag{13}$$

We recognize a band tridiagonal matrix on the left-hand side which can easily be inverted numerically to provide the new value of the velocity distribution at time $t + \mathrm{d}t$. Normalization of the velocity distribution is enforced at each time step.

Figure 2 shows a perfect agreement between the two methods, the iterative method allowing much higher precision to be reached (see the *y*-scale). The obtained distributions show strong deviations from the Gaussian, just as in the MD case. However, the distributions obtained by MD and DSMC agree only in the $\alpha \to 1$ limit, as was expected because of the spatial inhomogeneities appearing in the MD simulations.

The measure of the fourth cumulant $a_2$ (the first correction to the Gaussian) shows excellent agreement between the DSMC data and the kinetic theory predictions from equation (11),
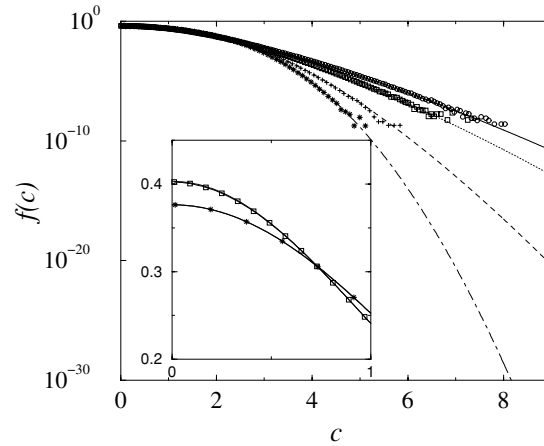
**Figure 2.** Velocity distributions obtained by DSMC with 25 000 particles (symbols) or by the iteration method (lines), in a log-linear scale, for restitution coefficients 0.1, 0.6, 0.9 and 0.99 (from top to bottom). Inset: same distributions on a linear scale, for restitutions 0.6 (stars) and 0.99 (squares).
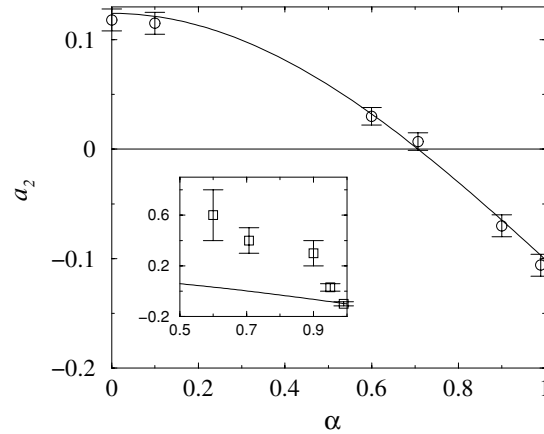


**Figure 3.** Values of the second Sonine coefficient $a_2$, obtained by measuring the fourth cumulant of $f(c)$ in DSMC simulations (circles), together with the kinetic theory prediction equation (11) (line). Inset: MD values for $a_2$ (squares) and kinetic theory prediction (line).

over the whole range of inelasticities (see figure 3). In the limit $\alpha \rightarrow 1$, $a_2$ obtained in MD coincides with the prediction of equation (11), namely, $a_2 \rightarrow -16/159$. Moreover, the full velocity distribution function coincides with that obtained in DSMC (see figure 5 below). However, as $\alpha$ decreases, the MD results significantly deviate from their molecular chaos counterparts (see the inset to figure 3)

Moreover, plotting the velocity distribution versus either $c^{3/2}$ or $c^3$, as in figure 4, shows that the high-energy tail obtained by the DSMC method has a shape going from the predicted $\exp(-Ac^{3/2})$ at large inelasticity to an $\exp(-Ac^3)$ behaviour at low inelasticity. For intermediate values of $\alpha$, a fit to a form $\exp(-Ac^B)$ would lead to intermediate values of $B$. Since the *real* high-energy limit *has to* follow an $\exp(-Ac^{3/2})$ law [4], this shows that
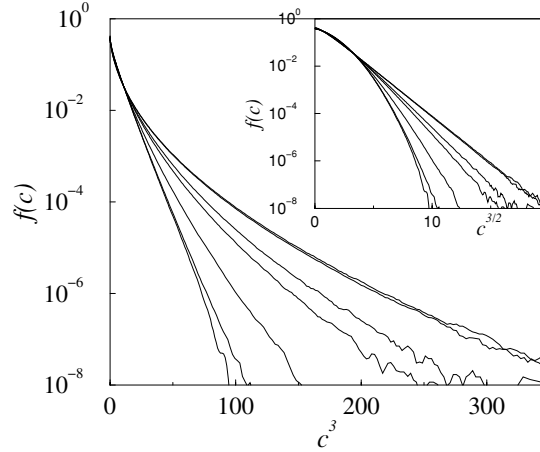
**Figure 4.** Velocity distributions, obtained by DSMC with 25 000 particles, versus $c^3$ and in the inset versus $c^{3/2}$, for restitution coefficients 0, 0.1, 0.6, 0.707, 0.9, 0.99 and 0.999 (from top to bottom): at low restitution coefficient, $f(c)$ shows an $\exp(-Ac^{3/2})$ behaviour, and an $\exp(-Ac^3)$ behaviour as $\alpha$ goes to 1.

for low $\varepsilon$, this limit is far beyond the reach of usual numerical methods, and emphasizes the fact that the range over which the large-$c$ limit is valid depends on the inelasticity. This is an important point since experiments have a limited precision, and the distribution function will have a practically vanishing weight long *before* this range is reached. In the next subsection we will see that the investigation of the $\alpha \to 1$ limit and the use of the iterative method allow us to understand the $\exp(-Ac^3)$ form obtained for $\alpha$ close to 1.

### 2.2. Small inelasticity limit

For small values of $\varepsilon \equiv 1 - \alpha$, the Boltzmann equation takes the form

$$\partial_t P(v, t) = D\partial_v^2 P(v, t) + n\varepsilon \int_{-\infty}^{\infty} \mathrm{d}w |v - w| P(w, t)$$

$$\times \left[ P(v, t) + \frac{1}{2}(v - w)\partial_v P(v, t) \right] + \mathcal{O}(\varepsilon^2). \tag{14}$$

The $\varepsilon \to 0$ limit can now be taken by introducing a scaled velocity $x = (n\varepsilon/D)^{1/3}v$. Using $x$, the Boltzmann equation yields an equation for the scaled distribution function $\phi(x) = (n\varepsilon/D)^{1/3} P_s(v)$ (where $P_s(v)$ is the stationary distribution $\lim_{t\to\infty} P(v, t)$):

$$\frac{\mathrm{d}^2\phi}{\mathrm{d}x^2} + \int_{-\infty}^{\infty} \mathrm{d}y |x - y| \phi(y) \left[ \phi(x) + \frac{1}{2}(x - y)\frac{\mathrm{d}\phi}{\mathrm{d}x} \right] = 0 \tag{15}$$

and we can integrate this equation twice to obtain

$$\phi(x) = C \exp\left\{ -\frac{1}{6} \int_{-\infty}^{\infty} \mathrm{d}y |y - x|^3 \phi(y) \right\}. \tag{16}$$

Here $C$ is a constant determined from the normalization condition $\int \mathrm{d}x \, \phi(x) = 1$. We have used the above equation to implement an iterative scheme to find numerically the corresponding
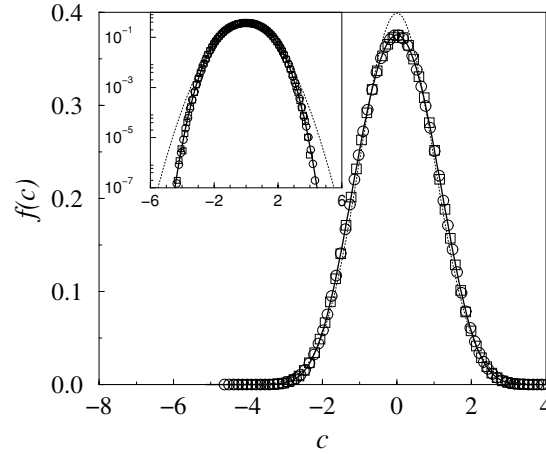
**Figure 5.** Symbols: velocity distributions obtained numerically at $\alpha = 0.999$ by MD and DSMC simulations; the solid line is the numerical solution $\phi(x)$ of equation (16), corresponding to the $\alpha \to 1$ limit, and here rescaled in order to have the same variance as the simulation data ($\langle c^2 \rangle = 1$). A perfect agreement between the three sets of data is observed. The dotted line is the Gaussian distribution.

velocity distribution. Moreover, as already pointed out in [13], one can easily see that the large $|x|$ limit is given by

$$\phi(x) = C e^{-\frac{1}{6}|x|^3} \tag{17}$$

while at small $x$, the function can be approximated by a Gaussian

$$\phi(x) = \tilde{C} e^{-\frac{1}{2}\lambda x^2} \tag{18}$$

with $\lambda = \int dx\,|x|\phi(x) \approx 0.785$ determined from the numerical solution of equation (16) and $\tilde{C} = C \exp\left(-\int dx\,|x|^3\phi(x)/6\right)$. The full numerical solution (displayed in figure 5) can also be investigated for locating the place where the crossover between the Gaussian and the $\exp(-|x|^3/6)$ type behaviour takes place. We find that the crossover range deduced from comparing the asymptotics (17) and (18), $x_{\mathrm{cr}} = 3\lambda \simeq 2.36$, is actually in agreement with numerical observations of the full function. Thus returning to non-scaled velocities, we can see that the crossover velocity $v_{\mathrm{cr}}^{(1)}$ diverges in the $\varepsilon \to 0$ limit as

$$v_{\mathrm{cr}}^{(1)} \approx \left(\frac{D}{n\varepsilon}\right)^{1/3}. \tag{19}$$

The important consequence of this result is that, for small dissipation, the $\exp(-Av^3)$ regime is reached for larger and larger velocities.

At large but finite velocities, an effective exponent can be defined by

$$n = \frac{\mathrm{d}}{\mathrm{d}\ln v} \ln \left\{-\ln \left[\frac{P(v)}{P(0)}\right]\right\} \tag{20}$$

corresponding to an apparent $\exp(-Av^n)$ behaviour. The values of $n$ for various inelasticities, obtained with the iterative method, are displayed in figure 6, together with the $\alpha \to 1$ limit. The effective exponent, starting from 2 at small velocities, increases and reaches a maximum at velocities that scale as $\varepsilon^{-1/3}$ for small $\varepsilon$ (as $v_{\mathrm{cr}}^{(1)}$). The height of the maximum, $n_{\mathrm{cr}}^{(1)}$, scales as $3 - n_{\mathrm{cr}}^{(1)} \sim \varepsilon^{1/3}$.
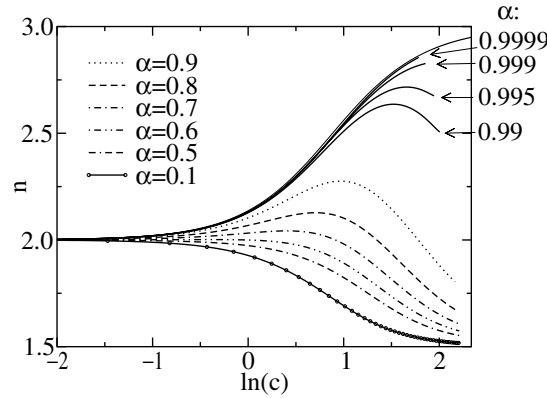
**Figure 6.** Effective exponent defined by equation (20) for the solution of the Boltzmann equation obtained by the iterative method and for the numerical solution of the $\alpha \to 1$ limit (upper curve, obtained from the iterative resolution of equation (16)).

One should note that the above scaling analysis explores only the $v \sim \varepsilon^{-1/3}$ range of the velocity space. As already mentioned, for any fixed $\varepsilon$, the large $v$ limit of the distribution function is a stretched exponential

$$P_s(v) \sim \exp\left\{-\frac{2}{3}\left(\frac{n}{D}\right)^{1/2}|v|^{3/2}\right\} \tag{21}$$

which is indeed observed numerically at relatively low values of $\alpha$ (see figure 4). Comparing the arguments of the exponents in (17) and (21), one finds a crossover scale diverging as

$$v_{\rm cr}^{(2)} \approx \left(\frac{D}{n\varepsilon^2}\right)^{1/3}. \tag{22}$$

The effective exponent displayed in figure 6 indeed decreases at velocities larger than $v_{\rm cr}^{(1)}$. For large inelasticities, the $n \to 3/2$ limit of large velocities is observed; however, since $v_{\rm cr}^{(2)} \approx v_{\rm cr}^{(1)}/\varepsilon^{1/3}$, it becomes impossible to observe the asymptotics (21) for small inelasticities, even for almost realistic values of $\alpha$, e.g. 0.95 (in experiments, $\alpha \sim 0.8$–0.9).

It has to be emphasized that this kind of behaviour is also observed in higher dimensions (for example, simulations of a two-dimensional heated granular gas with $\alpha = 0.8$ yield an almost Gaussian velocity distribution, even if the predicted high-energy behaviour is $\exp(-v^{3/2})$); it is therefore to be kept in mind for the comparisons of models with experiments in which the available precision often does not allow the predicted tails to be reached.

Finally, as already mentioned, it can be seen in figure 5 that, for $\varepsilon \to 0$, there is an excellent agreement between the single particle velocity distribution obtained in MD simulations (including both the space and velocity correlations) and that derived either from the asymptotic ($\varepsilon \to 0$) distribution function $\phi(x)$ or from the Monte Carlo simulation of the Boltzmann equation.

## 3. Freely cooling system

### 3.1. General considerations

In the freely cooling system, no energy is injected and the temperature is monotonically decreasing with time. The first investigations of the one-dimensional freely evolving gas were

undertaken in [6–9]; it was shown by molecular dynamics simulations that, depending on the values of the number of particles and the restitution coefficient, different instabilities could occur: e.g. at fixed number of particles $N$, if $\alpha$ is lower than a threshold, strong clustering occurs and leads to an inelastic collapse [6]. At larger $\alpha$, the instability develops more slowly, and the inelastic collapse is avoided. The temperature then decays according to the rate equation $dT/dt \propto -T^{3/2}$, i.e. $T(t) \sim t^{-2}$ [28], however derived for a homogeneous system, whereas strong heterogeneities develop in both velocity and space coordinates; a wavy, oscillatory in time, perturbation appears in a 'phase-space' plot (velocity versus position) [7, 8] with a tendency to form a bimodal velocity distribution.

The choice of a suitable quasi-elastic limit (where $\varepsilon \to 0$ and $N \propto 1/\varepsilon$ to avoid the inelastic collapse) leads to a simplified Boltzmann equation [7, 9–11], which can be understood using arguments from kinetic theory and hydrodynamics. This equation can be considered as formally exact as it has also been derived in [12] from the exact BBGKY-like hierarchy governing the evolution of the distribution [24]. In this quasi-elastic limit, the velocity was observed to develop a two-hump structure reminiscent of the bimodal velocity distribution observed in molecular dynamics [7, 9]. Moreover, exact results were derived in the context of the above-mentioned limit, where it was shown in particular that to leading order in $\varepsilon$, the velocity distribution consists of two symmetric Dirac peaks [12].

Extensive MD simulations were carried out in [19], using large sizes and probing large times, starting from a homogeneous situation with an initial given velocity distribution. As long as the system is homogeneous, the temperature decays according to $T(t) \sim t^{-2}$ [28]. As time evolves, space clustering of particles occurs and a $t^{-2/3}$ decay is obtained [19]. Since the number of particles is large, inelastic collapse should then occur; this catastrophic event is avoided by imposing that the collisions between particles with relative velocity smaller than a given threshold are elastic (they can equally be chosen to be sticky), and it was checked that the results do not depend on the chosen threshold. In this respect, the authors of [19] showed that the one-dimensional inelastic fluid belongs to the 'universality class' of the sticky gas, and advocated a mapping to the Burgers equation to describe the appearing heterogeneities. Moreover, at large times the rescaled velocity distribution $f(c)$ was found stationary and very close to a Gaussian up to the available accuracy (see also figure 7), even if the mapping to the Burgers equation predicts an $\exp(-Ac^3)$ high-energy tail. In fact, the bimodal structure of $f(c)$ reported in [7, 9] can also be observed in this case during the transient homogeneous behaviour, during which spatial heterogeneities and correlations build up, as shown in [29]; moreover, it can be clearly seen only by a convenient choice of the initial velocity distribution. The importance of spatial heterogeneities and correlations is emphasized in figure 7, where the rescaled velocity distribution obtained following the prescription put forward by Ben-Naim *et al* [19] (that is essentially Gaussian) is compared to that obtained from the homogeneous Boltzmann equation[5]. The two-hump structure displayed by the latter appears for $\alpha > 0.8$ and becomes more and more pronounced as $\alpha$ increases. In the next subsection, we will investigate in detail this structure in the $\varepsilon \to 0$ limit.

### 3.2. Small inelasticity limit

We have performed MD simulations using the two possibilities to avoid inelastic collapse mentioned in section 3.1.

- In figure 8, the top panel displays the results obtained for $\varepsilon = 5 \times 10^{-4}$ at various stages of the evolution: at first the system remains homogeneous but the tendency to form a

---

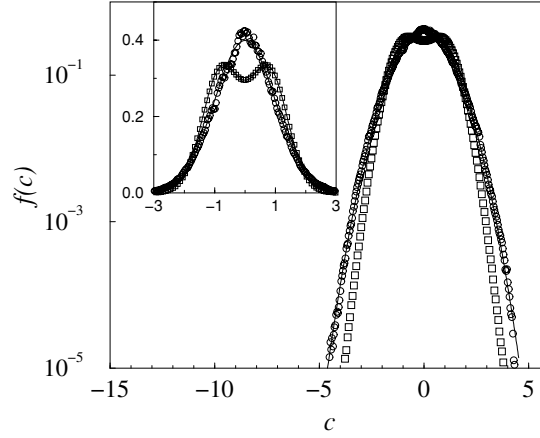[5] As expected, the temperature obeys the scaling law $T \propto t^{-2}$ in DSMC.

**Figure 7.** Rescaled velocity distributions at large times (in the scaling regime) at $\alpha = 0.85$ obtained by MD with $N = 25\,000$ (circles) and DSMC (squares) simulations. The solid line is the Gaussian distribution. In MD simulations, the inelastic collapse has been regularized by considering the same modified collision rule as in [19].

bimodal velocity distribution is rapidly obtained. The large time situation consists of two well defined clusters evolving with opposite velocities and yielding a sharply peaked bimodal velocity distribution (figure 8, bottom panel). In this case, the overall kinetic energy decay $E(t) \sim t^{-2}$ consists in a series of plateau since most of the dissipation occurs when the two clusters collide [7].

- On the other hand, with the regularization proposed in [19], the duration of the transient behaviour increases with $\alpha$, but the large time behaviour of the velocity distribution is always Gaussian.

It is striking to note that the above two procedures (small number of particles or elastic collisions at small enough velocities) lead to drastically different behaviour for the decay of the temperature, the spatial heterogeneities and the velocity distributions. Moreover it is remarkable that the homogeneous solution of the Boltzmann equation captures the bimodality of $f(c)$ (see figure 8, bottom panel) associated with a strongly heterogeneous system. In order to gain an insight into the approach to the limit $\varepsilon \to 0$, we devote the remainder of this paper to the analysis of the scaling properties of the homogeneous non-linear Boltzmann equation. We expect that for low enough inelasticity, $f(c)$ tends towards two delta peaks at $c = \pm 1$, as predicted in [12]. Performing DSMC simulations for smaller and smaller inelasticities allow this regime to be approached, and figure 9 shows how the peaks become narrower as $\alpha$ increases.

As the system cools, the velocity distribution $P(v, t)$ evolves into the Dirac distribution $\delta(v)$. The above numerical results indicate that this distribution actually consists of two peaks located symmetrically around the velocity origin, at positions decaying as $\pm(\varepsilon t)^{-1}$. Moreover, it appears that the results displayed in figure 9 for the rescaled velocity $c$ hide a self-similar structure, with the width of the peaks scaling as $\varepsilon^{1/3}$, as evidenced in figure 10 where the distributions corresponding to different inelasticities collapse onto a master curve. The characteristic features of this master curve are investigated below and to this end, we return to the $\varepsilon$ expansion of the Boltzmann equation (14), omitting the Fokker–Planck term $D\partial_v^2 P$, since the fluid evolves freely in the present situation.
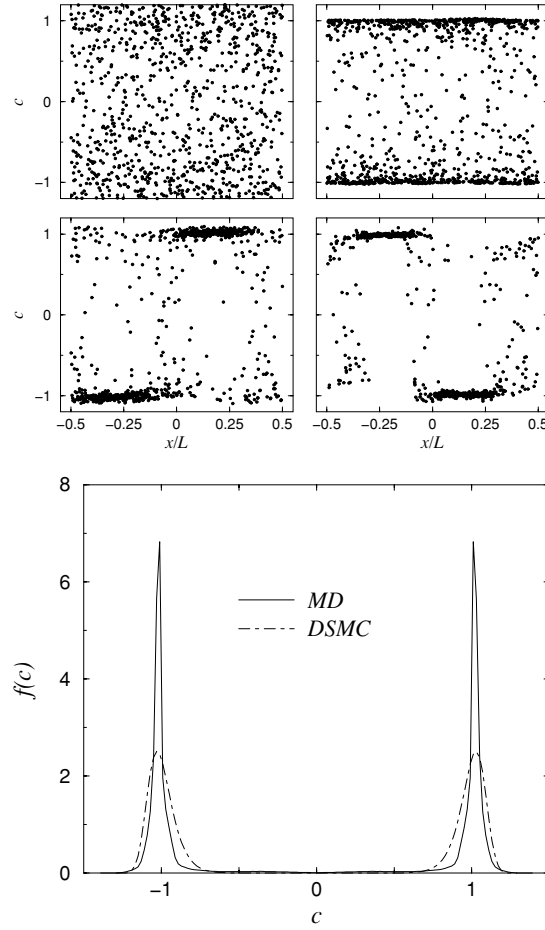
**Figure 8.** Top: velocity–density scatter plots obtained in MD simulations with $N = 1000$ and $\alpha = 0.9995$. Each dot marks the location of a particle in the $x$–$c$ plane, where $x$ denotes the position in the simulation box and $c$ denotes the velocity rescaled by the thermal velocity. Starting from an initial Gaussian distribution of velocities and random initial positions, the four snapshots correspond, from left to right and top to bottom, to four instantaneous configurations observed after respectively $4 \times 10^3$, $2 \times 10^4$, $4 \times 10^4$ and $6 \times 10^4$ collisions per particle. Bottom: velocity statistics obtained in MD by averaging in the late time regime for the same initial situation and parameters as above, compared to its 'mean-field' counterpart provided by DSMC simulations at the same inelasticity ($\alpha = 0.9995$).

From the evolution of temperature ($T \propto \varepsilon^{-2} t^{-2}$), it appears that a convenient scaling variable is $x \equiv n\varepsilon t v$ with a corresponding probability distribution function $\Phi$ related to $P(v, t)$ through $P(v, t) = n\varepsilon t \Phi(n\varepsilon v t)$. To leading order in $\varepsilon$, the Boltzmann equation is then brought into the simple form

$$\frac{\mathrm{d}(x\Phi)}{\mathrm{d}x} = \int \mathrm{d}y |x - y| \Phi(y) \left[ \Phi(x) + \frac{1}{2}(x - y)\frac{\mathrm{d}\Phi}{\mathrm{d}x} \right] \tag{23}$$

the solution of which reads [12]

$$\Phi(x) = \tfrac{1}{2}[\delta(x - 1) + \delta(x + 1)]. \tag{24}$$
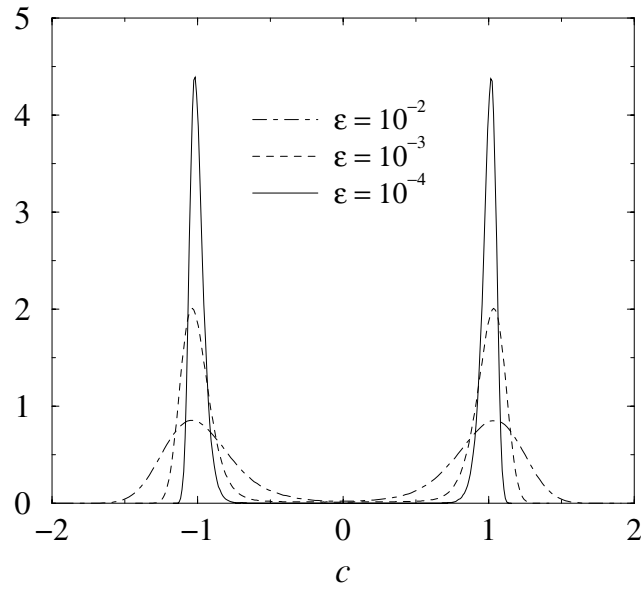
**Figure 9.** Rescaled velocity distributions at $\alpha = 1 - \varepsilon$ with $\varepsilon = 10^{-2}$, $10^{-3}$ and $10^{-4}$ obtained by DSMC simulations.
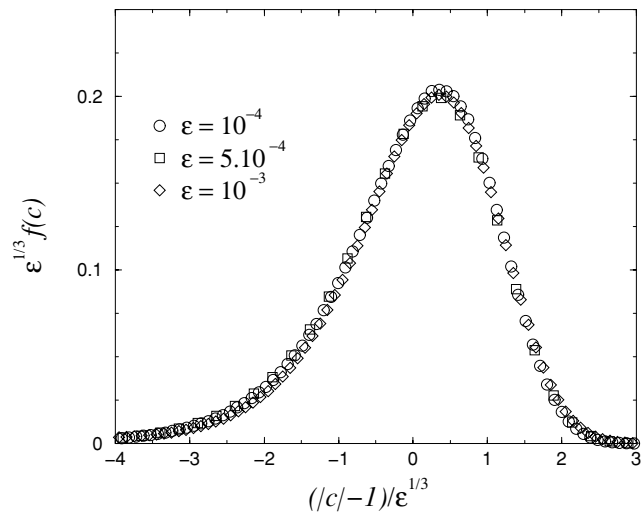


**Figure 10.** Self-similarity of the rescaled distribution functions for small inelasticities.

Looking for the self-similar structure of the peaks shown in figures 9 and 10 requires pushing the $\varepsilon$-expansion one order further compared to equation (23),

$$\frac{\mathrm{d}(x\Phi)}{\mathrm{d}x} = \int \mathrm{d}x' |x - x'| \Phi(x') \left[ \frac{1}{(1 - \varepsilon/2)^2} \Phi\left(x + \frac{\varepsilon}{2 - \varepsilon}(x - x')\right) - \Phi(x) \right] \qquad (25)$$

and considering solutions for $\Phi$ of the form

$$\Phi(x) = \varepsilon^{-\nu} \left[ \frac{1}{2} \psi \left( \frac{1 + b(\varepsilon)x}{\varepsilon^{\nu}} \right) + \frac{1}{2} \psi \left( \frac{1 - b(\varepsilon)x}{\varepsilon^{\nu}} \right) \right]. \tag{26}$$

In equation (25), the positive function $\psi$ has the interpretation of the ($\varepsilon$-rescaled) velocity distribution of left (or right) movers, and $b(\varepsilon) = b_0 + \varepsilon^{\nu} b_1 + \varepsilon^{2\nu} b_2$. Substituting the scaling assumption for $\Phi$ into (25) and performing the change of variables $x = -1 + \varepsilon^{\nu} y$, we obtain a non-linear integro–differential equation for $\psi(y)$:

$$a(\varepsilon)[\varepsilon^{1-\nu}(y\psi)' - \varepsilon^{1-2\nu}\psi'] = \frac{\varepsilon}{2} \int dy' |y - y'| \psi(y') \left( \psi(y) + \frac{1}{2}(y - y')\psi'(y) \right)$$

$$+ \frac{\varepsilon^{-\nu}}{2} \int dy' |2 - \varepsilon^{\nu}(y + y')| \psi(y')$$

$$\times \left[ -\varepsilon^{1-\nu}\psi' + \frac{\varepsilon}{2}(y + y')\psi' + \varepsilon\psi + \frac{1}{2}\varepsilon^{2-2\nu}\psi'' \right] \tag{27}$$

where terms of the form $\psi(-2\varepsilon^{-\nu} + y)$ have been neglected, anticipating that they will be exponentially small. Terms of order $\varepsilon^{2-2\nu}$ and $\varepsilon^{1+\nu}$ were equally neglected. Assuming again that $\psi$ will have a sharp decay, we write that under the integrals $|2 - \varepsilon^{\nu}(y+y')| = 2 - \varepsilon^{\nu}(y+y')$. Identifying on both sides of equation (27) terms of order $\varepsilon^{1-2\nu}$ and $\varepsilon^{1-\nu}$ leads, respectively, to

$$b_0 = \int dy' \psi(y') \tag{28}$$

which is the normalization condition, and

$$\psi'(y) \left\{ b_1 + \int dy' y' \psi(y') \right\} = 0 \tag{29}$$

which relates $b_1$ to $\langle y \rangle$ (a constant function $\psi$ cannot be a solution). We choose to impose $b_1 = -\langle y \rangle_{\psi} = 0$, where the notation $\langle \cdots \rangle_{\psi}$ stands for an average with respect to weight function $\psi$. Then one notices that the expansion is consistent only with the condition that the $\varepsilon^{2-3\nu}$ term can be cancelled by terms of order $\varepsilon$, which imposes that

$$\nu = \tfrac{1}{3} \tag{30}$$

and we recover the exponent $1/3$ that was needed to collapse the velocity distributions at several small inelasticities, as done empirically in figure 10. Finally we equate to zero the terms of order $\varepsilon$ to obtain the following integro–differential equation:

$$b_2 \psi'(y) = \int dy' \psi(y') \left[ \frac{1}{2} \psi(y)(|y - y'| - (y + y')) \right.$$

$$\left. + \frac{1}{4} \psi'(y)(|y - y'|(y - y') - (y + y')^2) + \frac{1}{2} \psi''(y) \right] \tag{31}$$

which we integrate once, remembering that $b_0 = \langle 1 \rangle_{\psi}$,

$$b_0 \psi'(y) + 2b_2 \psi(y) + \frac{1}{2} \psi(y) \int dy' \psi(y')(|y - y'|(y - y') - (y + y')^2) = 0. \tag{32}$$

We know from the direct analysis of the $\varepsilon \to 0$ limit of the scaling function that $b_0 = 1$, which we use from here on. At this stage we note that integrating the above equation and using $\langle y \rangle_{\psi} = 0$ leads to

$$2b_2 = \langle y^2 \rangle_{\psi}. \tag{33}$$

Conversely, setting $b_2 = \frac{1}{2}\langle y^2\rangle_\psi$ will automatically enforce $\langle y\rangle_\psi = 0$. We rewrite the equation for $\psi$ in the form

$$\ln \psi(y) = \ln C - 2b_2 y + \frac{1}{6}\int dy'\psi(y')[|y-y'|^3 - (y+y')^3]. \tag{34}$$

We now investigate the asymptotics of $\psi$. The left tail of the distribution at large negative values of $y$ reads

$$y \to -\infty \qquad \psi(y) \simeq C\exp\left[\frac{1}{3}y^3 + o(1)\right]. \tag{35}$$

This sharp decay at $y \to -\infty$ *a posteriori* justifies the approximations made in the course of the calculation. Note that omitting the first line on the rhs of equation (27) leads to exactly the same behaviour of the tail of the distribution. This has a physical interpretation: collisions between particles heading in the same direction can be neglected at large velocities. Opposite-velocity collisions are responsible for the form of the tail at large velocities. $o(1)$ represents contributions going exponentially fast to 0.

The right tail $y \to +\infty$ decays exponentially fast as

$$\psi(y) \simeq C'\exp\left\{-2\langle y^2\rangle_\psi y + o(1)\right\} \qquad \text{with} \qquad C' = C\exp\left\{-\frac{1}{3}\langle y^3\rangle_\psi\right\} \tag{36}$$

which again justifies the assumptions made so far. $o(1)$ again represents contributions going exponentially fast to 0. For completeness we mention the $y \to 0$ behaviour of the scaling function:

$$\psi(y) = C''\exp\left\{-\frac{y}{2}(3s^2 + |s|s\rangle_\psi + y^2\langle|s|\rangle_\psi) + \mathcal{O}(y^3)\right\} \qquad \text{with}$$

$$C'' = C\exp\left\{\frac{1}{6}\langle|y|^3 - y^3\rangle_\psi\right\}. \tag{37}$$

As a side remark, the integro–differential equation for $\psi$ can be cast in the form of an ordinary fourth-order differential equation

$$(\ln \psi)^{(iv)} = \psi. \tag{38}$$

Finally, we note that numerical iteration of the integro–differential equation (32) converges extremely rapidly. This allows us to determine the numerical constants $C$, $\langle y^2\rangle_\psi$ and $\langle y^3\rangle_\psi$ appearing in the asymptotics. The results obtained from this numerical scheme are compared with those of the DSMC method in figure 11, and show a quantitative agreement which improves as $\varepsilon$ is lowered in DSMC, as expected (see the dotted line at $\varepsilon = 10^{-4}$, closer to the asymptotic scaling form for $\psi$ than the dashed line corresponding to $\varepsilon = 10^{-3}$).

## 4. Conclusion

We have investigated the velocity statistics of one-dimensional granular fluids of inelastic particles with a particular emphasis on scaling properties in the elastic limit, both in the absence of an external forcing and in a system heated by random accelerations. For the heated system, we showed that the expected high-energy tail $\sim\exp(-Ac^{3/2})$ yields the correct asymptotic behaviour at finite inelasticity $\varepsilon$, but this asymptotics is masked by a tail $\sim\exp(-Bc^3)$ for $\varepsilon \to 0$, with the *rescaled* crossover velocity between the two regimes scaling as $\varepsilon^{-1/3}$. This shows that the limits of high velocity and low inelasticity do not commute: if $\varepsilon \to 0$ is taken *before* the high-energy limit, the distribution exhibits an asymptotic $\sim\exp(-Ac^3)$ large-$c$ behaviour:

$$f(\varepsilon, c) \stackrel{c\to\infty}{\propto} \exp(-A\,c^{3/2}) \qquad \text{for any } \varepsilon \neq 0 \tag{39}$$
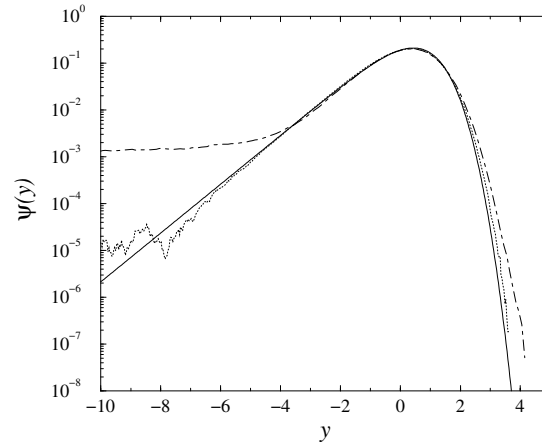
**Figure 11.** Comparison of the scaling function $\psi(y)$ (see text for definition) obtained within DSMC ($\varepsilon = 10^{-4}$, dotted line and $\varepsilon = 10^{-3}$, dashed line), with the solution of equaton (32) corresponding to the quasi-elastic limit.

whereas

$$\lim_{\varepsilon \to 0} f(\varepsilon, c) \stackrel{c \to \infty}{\propto} \exp(-Ac^3). \tag{40}$$

Thanks to a high-precision iterative scheme allowing the homogeneous non-linear Boltzmann equation to be solved, we could obtain the velocity distribution over 30 orders of magnitude at arbitrary $\varepsilon$, and thus define the apparent exponent $n$ of the stretched exponential law for large $c$ [$f(c) \propto \exp(-Cc^n)$]. However, even with such precision, the crossover between the two behaviours (39) and (40) is difficult to investigate (see figure 6).

For the freely evolving 1D granular fluid, we have investigated in detail the structure and scaling properties of the two-hump velocity distribution exhibited by the solution of the homogeneous cooling state of the Boltzmann equation, both numerically and analytically. Such a bimodal distribution captures an essential feature of the velocity distributions obtained in molecular dynamics simulations for parameters hindering the inelastic collapse (i.e. extremely small $\varepsilon$ or small systems). In this respect, a perturbative Sonine expansion in the spirit of that put forward in [4] fails at small $\varepsilon$, whereas such an expansion turned out to be remarkably accurate for the heated gas (see figure 3). In both cases it would predict a non-vanishing kurtosis correction $a_2$ for $\varepsilon \to 0$, which is a peculiarity of $d = 1$; as soon as $d > 1$, $a_2$ vanishes for small inelasticities, with or without forcing.

Given the striking features of the velocity distributions obtained in dimension 1, it would be of interest to perform the same analysis for realistic space dimensions $d > 1$, and to quantify more precisely space and velocity correlations [30], for both the heated and unforced systems, in order to understand in particular which of these features survive.

**Acknowledgments**

# References

[1]   Jaeger H M, Nagel S R and Behringer R P 1996 *Rev. Mod. Phys.* **68** 1259
[2]   Dufty J 2001 *Preprint* cond-mat/0108444
[3]   Williams D R M and MacKintosh F C 1996 *Phys. Rev.* E **54** R9
[4]   van Noije T P C and Ernst M 1998 *Gran. Matter* **1** 57
[5]   Peng G and Ohta T 1998 *Phys. Rev.* E **58** 4737
      van Noije T P C, Ernst M H, Trizac E and Pagonabarraga I 1999 *Phys. Rev.* E **59** 4326
      Henrique C, Batrouni G and Bideau D 2000 *Phys. Rev.* E **63** 011304
      Moon S J, Shattuck M D and Swift J B 2001 *Phys. Rev.* E **64** 031303
      Pagonabarraga I, Trizac E, van Noije T P C and Ernst M H 2001 *Phys. Rev.* E
      (Pagonabarraga I, Trizac E, van Noije T P C and Ernst M H 2001 *Preprint* cond-mat/0107570)
[6]   McNamara S and Young W R 1992 *Phys. Fluids* A **4** 496
[7]   McNamara S and Young W R 1993 *Phys. Fluids* A **5** 34
[8]   Goldhirsch I and Zanetti G 1993 *Phys. Rev. Lett.* **70** 1619
[9]   Sela N and Goldhirsch I 1995 *Phys. Fluids* **7** 507
[10]  Du Y, Li H and Kadanoff L P 1995 *Phys. Rev. Lett.* **74** 1268
[11]  Ramirez R and Cordero P 1999 *Phys. Rev.* E **59** 656
      Ramirez R and Cordero P 2001 *Granular Gases* ed T Poschel and S Luding (New York: Springer)
[12]  Benedetto D, Caglioti E and Pulvirenti M 1997 *Math. Mod. Num. An.* **31** 615
[13]  Benedetto D, Caglioti E, Carrillo J A and Pulvirenti M 1998 *J. Stat. Phys.* **91** 979
[14]  Brey J J, Ruiz-Montero M J and Cubero D 1996 *Phys. Rev.* E **54** 3664
[15]  Esipov S E and Pöschel T 1997 *J. Stat. Phys.* **86** 1385
[16]  Brey J J, Cubero D and Ruiz-Montero M J 1999 *Phys. Rev.* E **59** 1256
[17]  Montanero J M and Santos A 2000 *Gran. Matter* **2** 53
[18]  Huthmann M, Orza J A G and Brito R 2000 *Gran. Matter* **2** 189
[19]  Ben-Naim E, Chen S Y, Doolen G D and Redner S 1999 *Phys. Rev. Lett.* **83** 4069
[20]  Bernu B and Mazighi R 1990 *J. Phys. A: Math. Gen.* **23** 5745
[21]  Puglisi A, Loreto V, Marconi U M and Vulpiani A 1999 *Phys. Rev.* E **59** 5582
[22]  Cafiero R, Luding S and Herrmann H J 2000 *Phys. Rev. Lett.* **84** 6014
[23]  Allen M P and Tildesley D J 1987 *Computer Simulations of Liquids* (Oxford: Clarendon)
[24]  Résibois P and de Leener M 1977 *Classical Kinetic Theory of Fluids* (New York: Wiley)
[25]  Bird G 1976 *Molecular Gas Dynamics* (New York: Oxford University Press)
      Bird G 1994 *Molecular Gas Dynamics and the Direct Simulation of Gas Flows* (Oxford: Clarendon)
[26]  Biben T, Martin Ph A and Piasecki J 2002 *Physica* A, submitted
[27]  Landau L and Lifshitz E 1981 *Physical Kinetics* (Oxford: Pergamon)
[28]  Haff P K 1983 *J. Fluid Mech.* **134** 401
[29]  Baldassarri A, Marini Bettolo Marconi U and Puglisi A 2001 *Preprint* cond-mat/0111066
[30]  Soto R and Maréschal M 2001 *Phys. Rev.* E **63** 041303